LANGMUIR Article
Cite This: Langmuir 2017, 33, 11000-11009 pubs.acs.org/Langmuir

Determination of the Absolute Enantiomeric Excess of the Carbon Nanotube Ensemble by Symmetry Breaking Using the Optical Titration Method

Jinsook Sim, Somin Kim, Myungsu Jang, Minsuk Park, Hyunkyu Oh, and Sang-Yong Ju*

Department of Chemistry, Yonsei University, Seoul 03722, South Korea

Supporting Information

ABSTRACT: Symmetry breaking of single-walled carbon nanotubes (SWNTs) has profound effects on their optoelectronic properties that are essential for fundamental study and applications. Here, we show that isomeric SWNTs that exhibit identical photoluminescence (PL) undergo symmetry breaking by flavin mononucleotide (FMN) and exhibit dual PLs and different binding affinities (K_a). Increasing the FMN concentration leads to systematic PL shifts of SWNTs according to structural modality and handedness due to symmetry breaking. Density gradient ultracentrifugation using a FMN−SWNT dispersion displays PL shifts and different densities according to SWNT handedness. Using the optical titration method to determine the PL-based K_a of SWNTs against an achiral surfactant as a titrant, left- and right-handed SWNTs display two-step PL inflection corresponding to respective K_a values with FMN, which leads to the determination of the enantiomeric excess (ee) of the SWNT ensemble that was confirmed by circular dichroism measurement. Decreasing the FMN concentration for the SWNT dispersion leads to enantiomeric selection of SWNTs. The titration-based ee determination of the widely used sodium cholate-based SWNT dispersion was also demonstrated by using FMN as a cosurfactant.

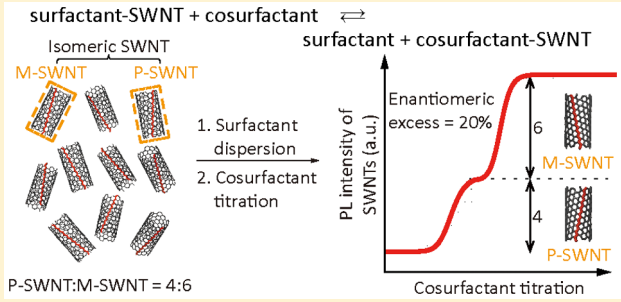

INTRODUCTION

Optoelectronic properties of single-walled carbon nanotubes (SWNTs) defined by a chiral (n,m) vector are extremely sensitive to symmetry-breaking structural deformations, such as axial, radial, or torsional strains.[1−3] The optical changes in the carbon nanotube upon strain have been widely investigated both theoretically[4] and experimentally,[5] which will be useful for electromechanical actuators[6,7] and sensors.[8] The strain of a SWNT has been controllably generated as a form of a polymer-embedded SWNT composite[7] or a stretching SWNT via an atomic force microscope tip,[2] inducing Raman and photoluminescence (PL) changes. As a consequence, deformation of the SWNT creates opposite optical shifts in the first (E_{11}) and second (E_{22}) transitions according to SWNT modality [i.e., mod 1 and mod 2 according to the remainder of $(n - m)/3$].[1,2,7]

On the other hand, an enantiomer is one of two isomeric chemicals that are nonsuperimposable mirror images of each other, and the enantiomeric excess (ee), which is defined by $|[R] - [S]|/([R] + [S]) \times 100$, where R and S denote the optically active right- and left-handed molecules, respectively, is a measure of its purity. The SWNT also has a mirror-image supramolecular enantiomeric structure with positive (P) or minus (M) helical handedness that originates from its hexagonal graphene symmetry,[9] and its isomer exhibits identical photoluminescence (PL). Peng et al. first demonstrated that handedness sorting of carbon nanotubes can be achieved by porphyrin isomers using circular dichroism (CD) measurement in which isomeric porphyrin selects equally isomeric SWNTs with identical absorption yet CD spectra with opposite signs.[10−13] More recently, other chiral molecules such as sodium cholate (SC)[14−17] and flavin mononucleotide (FMN)[18] have been shown to enable handedness sorting of SWNT. Interestingly, a chiral SC-based sorting scheme using density gradient ultracentrifugation (DGU)[15,19] alluded to the fact that optically active SC wrapping differentiates the SWNT isomer and results in slightly different absorption, CD, and densities of SWNTs for unknown reasons.

Among various methods, CD measurement with a known isomer concentration is used to determine the ee. In particular, determination of the ee of SWNTs requires a pure (n,m) SWNT because of the congested multiple optical transitions originating from SWNT heterogeneity.[17] Moreover, multiple optical transitions situated near visible and near infrared (IR) ranges demand long acquisition times for CD measurement. Thus far, the enantiomeric purity of the SWNT sample was obtained relatively by the normalized CD signal of the (n,m) SWNT with respect to the corresponding absorbance, which easily changed according to pH and environment.[7] Therefore, a general and facile method for defining the ee in the

Received: August 14, 2017
Revised: September 13, 2017
Published: September 19, 2017

DOI: 10.1021/acs.langmuir.7b02848
Langmuir 2017, 33, 11000−11009

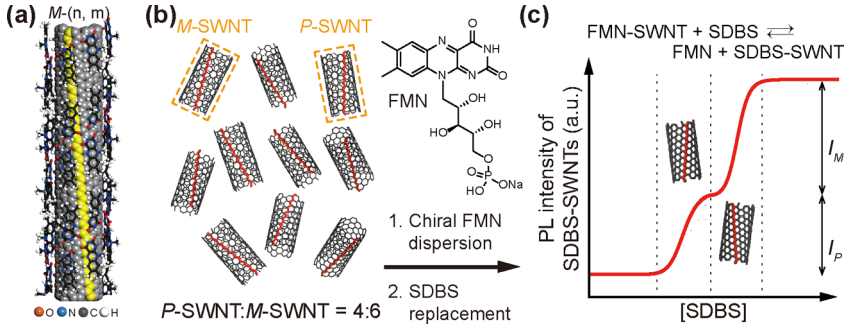

Figure 1. Handedness differentiation of SWNTs by surfactant exchange. (a) *P*-FMN helices around *M*-(*n*,*m*). Yellow lines on the acetylene line of SWNTs are drawn to indicate the rolling up direction of *M*-SWNT. FMN was replaced with 10-methyl isoalloxazine for the sake of visual clarity. (b) Schematic illustration of ee determination of the SWNT−FMN dispersion. (c) SWNT handedness is differentiated by chiral FMN wrapping and, upon SDBS replacement, exhibits two-step PL inflections (i.e., I_P and I_M), corresponding to less stable *P*-SWNT and more stable *M*-SWNTs, according to the increasing SDBS concentration.

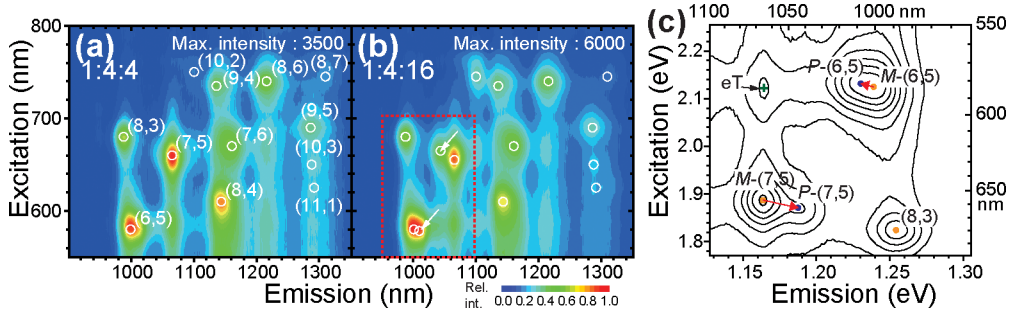

Figure 2. Bimodal PL peak of SWNTs with FMN. (a and b) PLE maps of SWNTs from 1:4:4 and 1:4:16 dispersion samples, respectively. PL positions of each chiral nanotube are marked with a circle. (c) Close-up maps of the red dotted box in panel b on an electronvolt scale. *P*-(*n*,*m*) peaks (blue) are displayed together with the PL positions of *M*-(7,5) and *M*-(6,5) (red). The green cross represents an energy transfer (eT) peak from (6,5) to (7,5) chiralities.

heterogeneous SWNT sample is necessary to evaluate the purity of the sorted SWNT and thus accurately describes the SWNT according to its chirality and handedness.

As described below, we find that isomeric SWNTs that exhibit identical optical transitions undergo symmetry breaking by FMN and exert slightly different PLs, resulting in the determination of ee value of various SWNTs at once. Handedness differentiation of a SWNT is enabled by FMN, which results in slightly different optical transitions of the SWNT according to handedness and modality, because of electronic structure modification by the FMN strain. Those FMN−SWNT interactions further lead to the different binding affinity according to SWNT chirality, handedness, and concentration, probed by optical titration assays with a cosurfactant. Upon cosurfactant replacement, nearly all SWNTs exhibit two-step PL trajectories, which enable us to calculate the absolute ee value of the SWNT isomer. Furthermore, the ee values of SWNTs dispersed by SC, the most frequently used surfactant for SWNT sorting, are determined using surfactant exchange with FMN.

RESULTS AND DISCUSSION

FMN [a phosphate analogue of vitamin B_2 (Figure 1b)] has a chiral D-ribityl phosphate side chain and can assemble on atomically flat carbon[18,20−22] and other nanomaterials.[23] In the central scheme, as shown in Figure 1a, the stability of the FMN−SWNT assembly is maintained by the balance of three forces: (i) $\pi-\pi$ interaction between the FMN helix and isoalloxazine ring up to 2 eV,[24] (ii) cooperative quadruple hydrogen bonding (H-bonding) of isoalloxazine moieties between antiparallel FMN helices, and (iii) ionic stability from the D-ribityl phosphate group[20] enabling and directing the *P*-helical FMN assembly shape due to electrostatic interaction between the D-ribityl and isoalloxazine moiety.[18] Using the cooperative interplay, FMN possesses chirality[20] and *M*-handedness[18] selection abilities for SWNTs.

Panels b and c of Figure 1 delineate schematics of SWNT ee determination described in this study. A SWNT dispersion wrapped in chiral FMN contains both optical isomers. Initially, the *P*-FMN helix has different relative binding affinities with underlying SWNT isomers and, upon exchange with an achiral surfactant such as sodium dodecylbenzene sulfonate (SDBS), reveals two distinct PL steps originating from the SWNT isomer.

Dual PL of Single Chiral SWNTs. FMN−SWNT dispersions were prepared by sonication of a mixture of 1 mg of HiPco SWNTs, 4 mL of water, and varying FMN concentrations [i.e., 1, 2, 4, 16 mg, etc. (which is termed the 1:4:*X* protocol for each varying FMN concentration)]. Subsequent centrifugation at 20000*g* for 2 h was conducted to collect the FMN−SWNT supernatant according to the reported method.[18,20,25] The resulting absorption spectra (Figure S1) and photoluminescence excitation (PLE) maps of FMN−SWNT dispersions (Figure S2a−g) show that the SWNT sample has well-resolved first (E_{11}, 950−1350 nm) and second (E_{22}, 600−900 nm) semiconducting optical transitions of HiPco SWNTs.[26] The E_{11} and E_{22} of the FMN−SWNT dispersions are red-shifted compared to

DOI: 10.1021/acs.langmuir.7b02848
Langmuir 2017, 33, 11000−11009

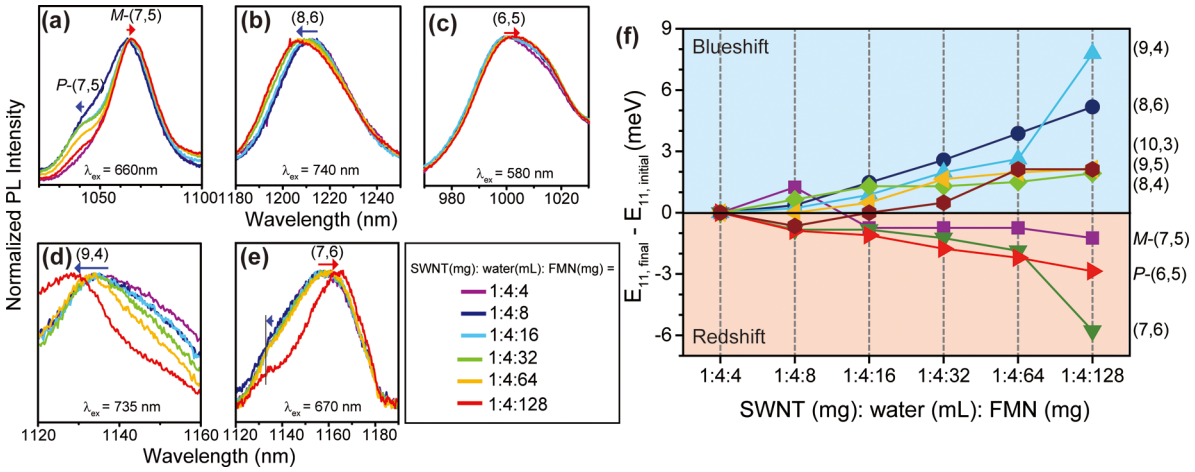

Figure 3. Intensity-normalized PL position shift of SWNT chirality according to increasing FMN and SWNT concentrations. λ_{ex} denotes the excitation wavelength. (a–e) PL position shifts of SWNT chirality. (f) Difference in energy between the initial E_{11} and final E_{11} with increasing FMN dispersion.

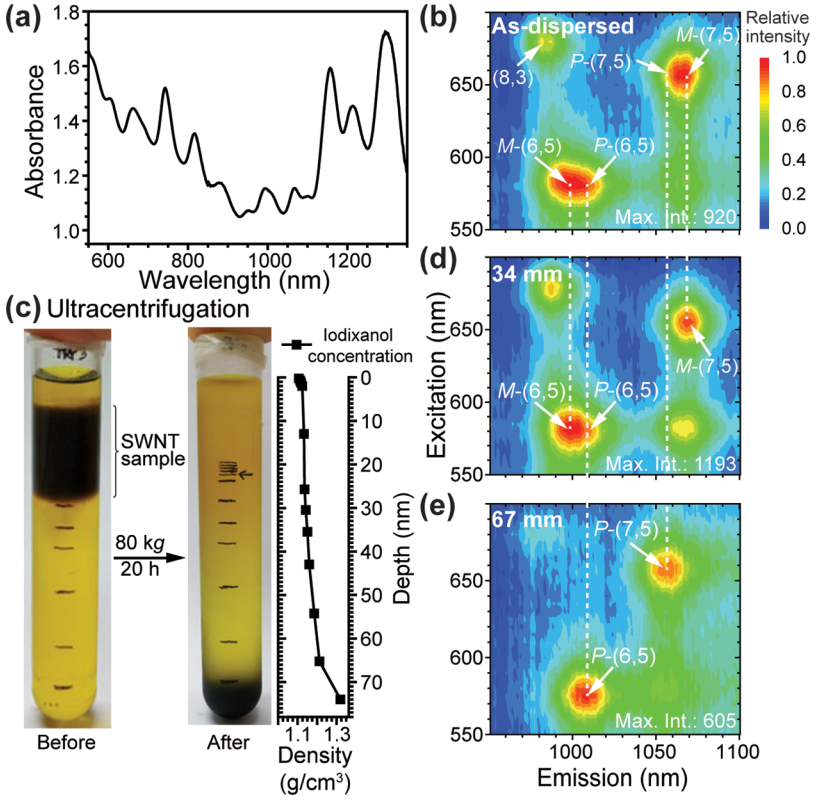

Figure 4. PL position and density difference of *P*- and *M*-SWNTs determined by the DGU method. (A) UV–vis–NIR absorption spectrum and (B) resulting PLE map of the FMN–HiPco dispersion. (C) Photographs before and after ultracentrifugation of the FMN–SWNT dispersion. PLE maps at depths of (d) 34 and (e) at 67 mm from the meniscus.

absorption and PLE spectra from SDS-dispersed SWNTs[26] due to π–π interaction between FMN and SWNT.[20]

Drastic chirality-associated dual PL peaks of SWNTs were observed when the dispersion was acquired with more FMN. To understand the effect of increased FMN and SWNT concentrations, we compared the representative, "low-concentration" (i.e., 1:4:4 protocol) and "high-concentration" (i.e., 1:4:16 protocol) FMN–SWNT dispersion samples. The PLE map from a low-concentration sample (Figure 2a) exhibits a total of 11 SWNT PL peaks (white circles).[20] Here, we assigned the initial (*n*,*m*) chirality of the low-concentration sample as *M*-SWNT because the FMN–HiPco dispersion with the same protocol produces an *M*-enriched sample.[18] Interestingly, the PLE map from the high-concentration sample (Figure 2b) reveals that certain chiral nanotubes, including (7,5) and (6,5), have new PL peaks [termed *P*-(7,5) and *P*-(6,5), indicated by white arrows in Figure 2b], on top of the initial PL peaks [i.e., *M*-(7,5), and *M*-(6,5)] having the same PL position of the low-concentration sample. The enlarged contour map on an electronvolt scale (Figure 2c) shows that the PL position of *P*-(7,5) is separated from that of the *M*-(7,5) peak, whereas that of the *P*-(6,5) nanotube overlaps the *M*-

DOI: 10.1021/acs.langmuir.7b02848
Langmuir 2017, 33, 11000–11009

(6,5) PL. The increase in the intensity of the *P*-(6,5) PL peak is clearly seen in a series of PLE maps from SWNT dispersions with an increasing FMN concentration (Figure S2a–g with an increasing FMN concentration in the protocols), suggesting that an increased *P*-(6,5) concentration originates from an increased SWNT concentration. These double PL peaks are not from the exciton (bound electron–hole pair) energy transfer (eT) peaks[27] (green cross in Figure 2c) formed at the PL cross points between larger and smaller bandgap nanotubes, or from the electron–phonon interaction peak,[28] which is typically observed at 200 meV beside the PL peaks. E_{11} and E_{22} of the *P*-(7,5) peak are positioned at 27 and −28 meV, respectively, as compared to those of the low-concentration *M*-(7,5) peak. Meanwhile, the *P*-(6,5) nanotube shows the opposite trend (i.e., − 9 and 7 meV shifted in both E_{11} and E_{22}, respectively), compared to the *M*-(7,5) case.

Such a dual PL trend became obvious as the FMN concentration increased. For this, we tracked PL positions of several SWNT chiralities with an increasing FMN concentration up to 128 mg in the protocol. The E_{11}-normalized PL spectra of several (*n*,*m*) SWNT chiralities excited at the ~E_{22} wavelength[20] are shown in Figure 3a–e (see Figure S3 for the remaining SWNT chiralities). According to the nanotube chirality, an increasing FMN concentration results in various E_{11} shift behaviors. Several nanotubes such as the (7,5) tube (Figure 3a) have two distinct PL positions, while other nanotubes display a progressive PL red-shift [i.e., (6,5) and (7,6)] or blue-shift [i.e., (8,6) and (9,4)] as compared to the initial E_{11}. It is worth noting that *P*-(7,5) was initially not present for the 1:4:4 protocol, and its PL intensity increased with increasing FMN concentration protocols because of the enantiomeric selection of *P*-FMN to *M*-SWNT at lower FMN concentrations.[18] Figure 3f displays the difference in energy between initial and final E_{11}'s with increased FMN dispersion. With an increase in the FMN concentration and a concomitant increase in the SWNT concentration, a SWNT having mod 2 [i.e., (9,4) and (8,6)] displays a blue-shift whereas a SWNT having mod 1 exhibits a red-shift [i.e., (6,5) and (7,6)]. Some SWNTs such as (9,5) and (8,4) display a relatively small PL blue-shift of <2 meV. This trend suggests the first indication that the modality and handedness of SWNT are linked together for the PL change. To pinpoint the net effect of increasing the FMN concentration on SWNT PL, more FMN was simply added to the 1:4:4 protocol containing a fixed amount of SWNT. PL spectra of each of the SWNT chiralities (Figure S4) show small or nearly no changes as compared to the trend mentioned above. This comparison suggests that an increase in the SWNT concentration is the main contributor to such a PL shift. Together with *M*-SWNT enrichment in the low-concentration sample,[18] this suggests the increased *P*-SWNT level for the PL shift.

Clear evidence that SWNT wrapped by FMN has two distinct PL positions was obtained via a DGU experiment (see the Supporting Information for a detailed experiment). The high-concentration FMN–SWNT sample was prepared according to the method previously reported.[29] The ultraviolet–visible–near-infrared (UV–vis–NIR) absorption spectrum of the resulting dispersion (Figure 4a) displays well-resolved E_{11} and E_{22} of FMN–SWNT dispersions. The initial PLE map (Figure 4b) displays an ovalish PL peak at positions (6,5) and (7,5). Upon ultracentrifugation, the initial dark FMN–HiPco sample band as shown in Figure 4c disappeared and displayed only the bundled sample at the bottom of the centrifugation tube of >70 mm. Using a custom-made translational stage that allows us to probe PLE maps along the centrifugation tube described elsewhere (see the Supporting Information),[29] we obtained PLE maps at depths of 34 and 67 mm whose isopycnic densities correspond to 1.15 and 1.24 g/mol, respectively. While the PLE map at 34 mm shows PL peaks originating from *M*-(6,5) and *M*-(7,5) PLs, the map at 67 mm displays PLs from the opposite handedness [i.e., *P*-(6,5) and *P*-(7,5) PLs]. Moreover, *P*-SWNT structures are situated at a higher density, while *M*-nanotubes are positioned at lower densities. It should be noted that DGU results in nanotubes with a smaller diameter at a lower isopycnic density because of the hydration volume of the surfactant.[30,31] Importantly, this finding suggests that the construct of FMN and the SWNT isomer not only has different PL positions but also indicates different diameters (i.e., the *M*-tube has a diameter smaller than that of the *P*-tube). Moreover, a SWNT having mod 1 [i.e., (6,5)] and mod 2 [i.e., (7,5)] has different E_{11} shift responses according to the handedness of SWNT, similar to those witnessed in dual PL observation. While *M*-(6,5) displays blue-shifted E_{11} (Figure 4d) compared to that of *P*-(6,5) at greater depths (Figure 4e), (7,5) exhibits the opposite trend according to handedness.

The question of what differentiates optical transitions of SWNTs arises. We ascribed such a trend to the unidirectional torsion of SWNTs by *P*-FMN assembly (Figure 1a).[18,32] More FMN on SWNT would cause structural deformation by wringing SWNTs. To understand this behavior, the band structure of a SWNT must be discussed. Tight binding calculation of SWNT[9] produces a conduction band (CB) and a valence band (VB) along the reciprocal lattice depicted in Figure 5a. In particular, a Dirac cone indicated by the circled

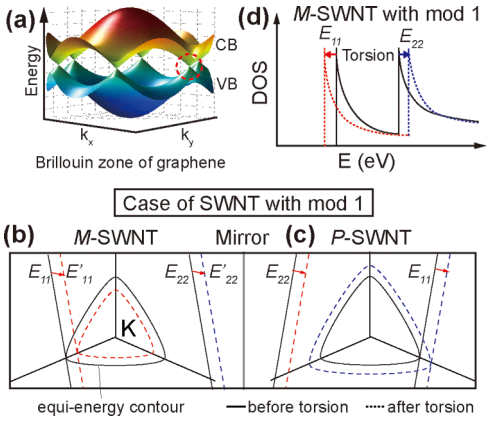

Figure 5. Modality- and handedness-dependent E_{ii} changes of SWNTs in the Brillouin zone. (a) Energy dispersion according to reciprocal lattice k_x and k_y. CB and VB denote conduction and valence bands, respectively. Case of SWNT with mod 1. Optical transition changes of (b) *M*-SWNT and (c) *P*-SWNT according to unidirectional torsion (red arrows). (d) Resulting optical transition shifts of *M*-SWNT with mod 1.

region is formed at the K point of the Brillouin zone that touches the CB and VB. Because of the quantum confinement imposed by the SWNT diameter, parallel E_{11} and E_{22} wavevectors (Figure 5b) are formed near the K point whose energy is proportional to the distance to the K point and is further affected by a trigonal warping effect.[33] Because *M*- and *P*-SWNT have mirror-image energy contour maps (panels b and c of Figure 5, respectively), unidirectional lattice

DOI: 10.1021/acs.langmuir.7b02848
Langmuir 2017, 33, 11000–11009

deformation of SWNT with mod 1 results in an E_{11} red-shift and an E_{22} blue-shift for the M type, whereas that leads to an E_{11} blue-shift and an E_{22} red-shift for the P type. Opposite optical transition changes occur for M-SWNT with mod 2 (Figure S5a,b). Summarized relative E_{11} shifts according to handedness and modality are listed in Table 1, and the opposite trend is seen for the E_{22} shift. Although the qualitative change in the behavior of PL positions is similar to that of the SWNT–polymer composite under uniaxial stretching,[7] FMN-induced PL changes leave dual PL from the SWNT isomer due to unidirectional strain.

Table 1. Optical Transition Changes According to Handedness and Modality of SWNTs

SWNT		
handedness	modality	relative E_{11} as compared to that of another isomer
M	1	blue-shift
	2	red-shift
P	1	red-shift
	2	blue-shift

Binding Affinity-Based ee Determination. The origin of the observed new PL peak was obtained by measuring the relative binding affinity of chiral SWNTs with FMN. It has been shown that chiral FMN on SWNTs is replaced by achiral SDBS[20] and other surfactants,[18,25] which is useful for probing the binding affinity between the surfactant and SWNTs. A series of PLE maps of FMN-wrapped nanotube samples using the 1:4:16 protocol was acquired by the addition of ≥25 μM SDBS (see Methods), and selective maps (i.e., 0.0, 0.6, and 1.5 mM) are presented in Figure 6a. As the concentration of SDBS increases, the PL intensity of FMN-wrapped (8,4) tubes (white lines across the PLE maps) completely disappears while a blue-shifted PL position that originated from a SDBS-wrapped (8,4) nanotube emerges, indicating successful replacement of FMN with SDBS on SWNTs due to a local dielectric environment change.

Such trends in PL intensity from FMN- and SDBS-derived SWNTs positions are tracked to display the PL intensity trajectories as red and blue. Panels b and c of Figure 6 are such examples of (8,4), and (7,5) chiralities, respectively (see Figure S6a–i for the nine remaining nanotubes) according to increasing FMN protocol from top to bottom plots (i.e., 1:4:1, 1:4:4, and 1:4:16 protocols, respectively). The PL intensity traces of (8,4) nanotubes from FMN- and SDBS-wrapped SWNTs of the 1:4:1 protocol (top of Figure 6b) show that the PL intensity trajectories from FMN- and SDBS-wrapped (8,4) tubes at the same SDBS concentration are complementary to each sigmoidal transition. The midpoint of sigmoidal transitions of the PL intensity curve from each nanotube can be described as a relative affinity K_a of FMN for SWNTs against SDBS by the Hill equation (see Methods).[20] Special care was taken to fit Hill curves to experimental plots, in

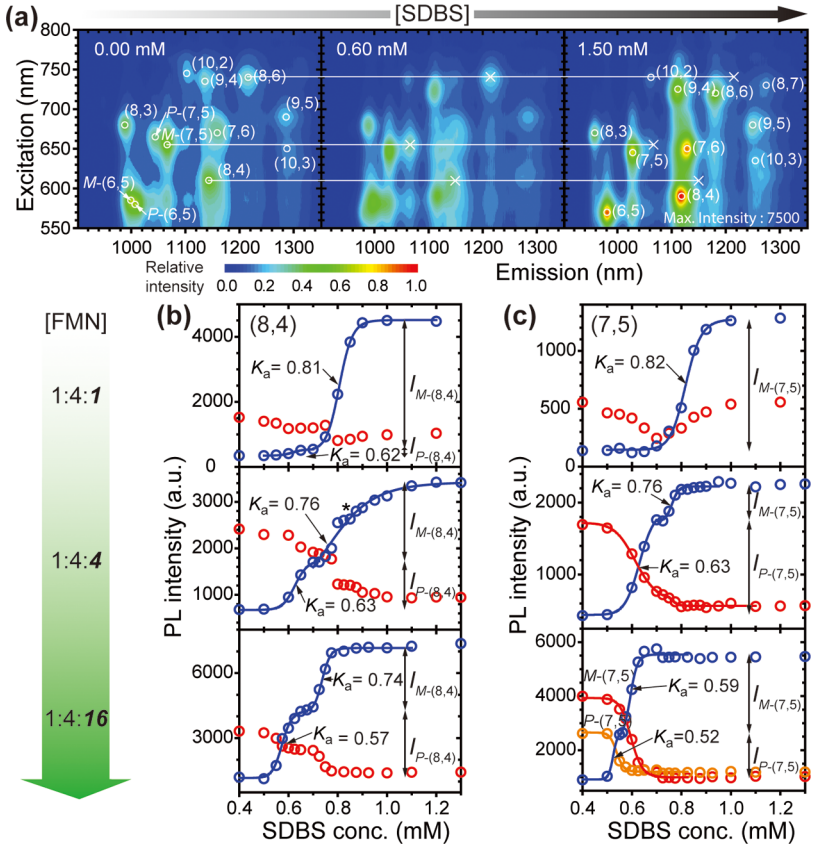

Figure 6. Differences in K_a in various SWNTs and origin of P-SWNT. (a) Series of representative PLE maps from the 1:4:16 FMN–SWNT sample with an increase in SDBS concentration (0.00, 0.60, and 1.50 mM from left to right, respectively). SWNT PL intensities from (b) (8,4) and (c) M-(7,5) and P-(7,5) from 1:4:1 (top), 1:4:4 (middle), and 1:4:16 (bottom) protocols. SDBS– and FMN–SWNT-derived PL intensities are marked as blue and red circles, respectively. Orange circles denote P-(7,5). An asterisk on the curve indicates an artifact that originated from the adjacent PL transitions.

DOI: 10.1021/acs.langmuir.7b02848
Langmuir 2017, 33, 11000–11009

which two sigmoidal curves have been drawn only when both PLs of FMN- and SDBS-suspended SWNT are complementary to each other. The PL intensity trajectory is best described by two-step Hill curves (blue) with K_a values of 0.62 ± 0.008 and 0.81 ± 0.001 mM, denoted as *P*-(8,4) and *M*-(8,4), respectively. Attempts to fit with a single Hill curve result in a larger standard deviation in K_a (data not shown). The further increased FMN protocols (i.e., 1:4:4 and 1:4:16 in the middle and bottom panels of Figure 6b, respectively) result in clear two-step sigmoidal replacement with distinct patterns: (i) the K_a values of each sigmoidal curve decrease with increased FMN protocols, and (ii) the PL intensity ratio of *M*-(8,4) and *P*-(8,4) steps nearly becomes unity with a higher FMN protocol such as 1:4:16. The other seven nanotubes also exhibited a universal two-step PL trend during titration (Figure S6a–i), except that the nanotube PL intensities [i.e., (10,2) and (8,7)] were within the noise level.

The K_a value indicates stabilization degree of FMN–SWNT in the dispersions.[20] The question is why an increased FMN concentration causes less stable FMN–SWNT in the dispersions. We ascribe this to the aforementioned helical torsion on SWNTs exerted by the increased FMN concentration (Figure 1a): to wring the nanotube, the FMN helix first grabs nanotubes through its H-bonding and the increased FMN concentration results in helical torsion and makes SWNT twisted. The helical torsion would result in weakened $\pi-\pi$ interaction between the isoalloxazine ring and graphene side walls. The destabilization is evident from the decreased K_a of nearly all SWNTs at high FMN concentrations (see Table S2 for K_a values according to SWNT chiralities and dispersion protocols).[34]

Similarly, two sigmoidal steps were also observed for (7,5) nanotubes showing *M*- and *P*-PL peaks. While the 1:4:1 sample (top panel of Figure 6c) displays a single sigmoidal step, the 1:4:4 sample (middle) displays two-step inflections of PL intensity, like the case of the (8,4) tube. In the 1:4:16 sample, separated *M*-(7,5) (red) and *P*-(7,5) (orange) PL trajectories of the FMN case were observed, which displays a single sigmoidal transition with K_a values of 0.52 ± 0.002 and 0.59 ± 0.004 mM, respectively. Simultaneously, the achiral SDBS-wrapped (7,5) tube displays the two increased PL steps at one PL position, with K_a values identical to that of each of the FMN-wrapped *P*-(7,5) and *M*-(7,5) tubes. It is noteworthy that the intensity ratio of FMN-derived $I_{M\text{-}(7,5)}$ to $I_{P\text{-}(7,5)}$ is nearly same as those of SDBS-wrapped (7,5). This result indicates that the *P*-(7,5) peak originates from the other handedness of the (7,5) tube, resembling the handedness signature of SWNTs produced by density gradient ultracentrifugation.[15]

To pinpoint whether the two steps originate from the handedness of SWNT, CD spectra from *M*-(*n*,*m*) and *P*-(*n*,*m*) portions were measured. Figure 7a exhibits the PL intensity profile of titration of FMN-(8,6) against SDBS, showing two K_a values at 0.71 and 0.98 mM. Sample 1 (green bar above Figure 7a) is expected to be an enantiopure (8,6) sample. After FMN removal steps (see Methods), (8,6) enrichment to >86% purity was confirmed by PLE mapping (Figure S7a). CD and absorption spectra (green traces in panels b and c of Figure 7) suggest that sample 1 is enriched with *M*-(8,6) based on the positive sign of E_{22} at 730 nm in the CD trace, whereas sample 2 has much weaker CD signals. Although it has a background-subtracted absorbance (~0.03) similar to that of sample 1, sample 2 (black bar) containing both handedness types displays an ~4-fold smaller E_{22} CD signal from *M*-(8,6) due to the larger abundance ratio of $I_{M\text{-}(8,6)}$ to $I_{P\text{-}(8,6)}$ (Figure 7a). This explains the ~18% ee of sample 2 listed in Table S2, which will be discussed below. The magnitude of E_{22} in the CD spectrum exhibits an optical isomer purity 20-fold greater than that reported elsewhere, based on the relative CD/background-subtracted absorbance ratio.[16]

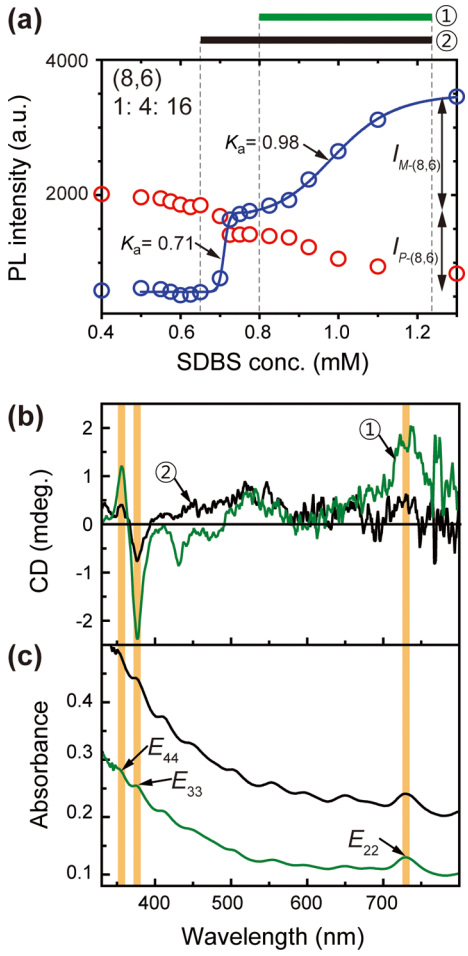

Figure 7. CD measurement from different isomeric ratio samples. (a) PL intensity of the (8,6) nanotube from 1:4:16 protocols upon SDBS titration. The upper color codes represent samples 1 and 2 collected for CD and optical measurements. Corresponding, color-matching (b) CD and (c) absorption spectra from each sample indicated in panel a.

Because achiral SDBS-wrapped SWNT isomers display identical PL positions and intensities, each sigmoidal PL step was used to measure the ee using the following established equation:

$$\text{ee} = |I_{M\text{-}(n,m)} - I_{P\text{-}(n,m)}|/[I_{M\text{-}(n,m)} + I_{P\text{-}(n,m)}] \times 100 \quad (1)$$

where $I_{P\text{-}(n,m)}$ and $I_{M\text{-}(n,m)}$ denote the initial and later PL counts, respectively (see Table S2 for ee values according to nanotube chiralities and various sample protocols). Among 11 nanotubes, two nanotubes display two separate PL peaks originating from both handedness types, and eight nanotubes display two sigmoidal PL traces from one PL peak during SDBS titration.

Figure 8a shows the plot of K_a versus nanotube chirality and handedness (i.e., + and − for *P*- and *M*-SWNT, respectively) according to different protocols. Among four different protocols, the 1:4:2 protocol displays the highest K_a value for all chiral nanotubes, indicating that this protocol has the optimal FMN configuration exhibiting the highest affinity for

DOI: 10.1021/acs.langmuir.7b02848
Langmuir 2017, 33, 11000–11009

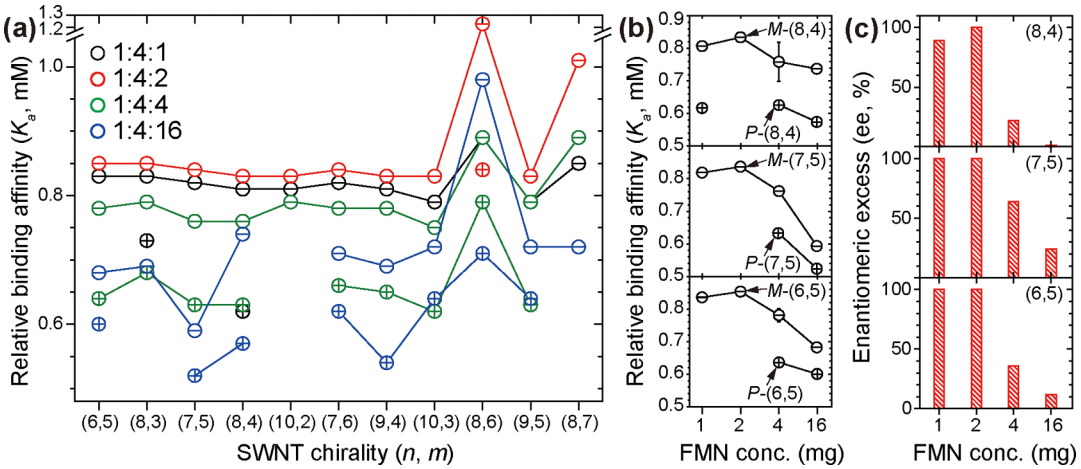

Figure 8. Variation of ee according to nanotube chirality, handedness, and dispersion protocol. (a) Overall trends of K_a according to nanotube chirality, handedness (+ and − for *P*- and *M*-SWNT, respectively), and sample protocol. (b) Plot of the resulting relative binding affinity (K_a) of FMN−SWNT dispersions [i.e., (8,4), (7,5), and (6,5) tubes] against SDBS titration with an increasing FMN concentration in sample protocols. (c) Corresponding ee values according to sample protocol.

SWNTs. In general, with the exception of (8,6) tubes, chirality-derived variation in K_a is not greater than handedness variation. In addition, the K_a difference in handedness in the 1:4:16 protocol varies significantly according to nanotube chirality compared to that in the 1:4:2 protocol, suggesting the enhanced van der Waals interaction as a result of crowded FMN on the SWNT surface. The top panel of Figure 8b shows the K_a variation of (8,4) according to handedness and FMN concentration. K_a values decrease with a steeper slope on both sides for the 1:4:2 protocol, which is also true for other chiral SWNTs (other plots in Figure 8b and Table S2). Figure 8c shows the ee trends of (8,4), (7,5), and (7,6) SWNTs, in which tubes from the 1:4:2 protocol display ee values of almost 100% and those from the 1:4:16 protocol rapidly decrease to <20%. This trend also occurs for other nanotubes (Table S2) and is attributed to the FMN concentration that is high enough to accommodate both SWNT handedness types. Nearly half of the FMN−SWNT chiralities exhibit an ee of <20% in the 1:4:16 protocol, leading to a racemic mixture of SWNTs at higher FMN concentrations.

This method is not limited to determination of the enantiomeric purity of SWNTs wrapped by FMN. A HiPco dispersion using 1 wt % SC, the most widely used surfactant for SWNT sorting in DGU[14,15,31] and sephacryl gel,[16,17,35,36] was prepared for general applicability of the ee determination method (see Methods). At this time, we utilized FMN instead of SDBS as a titrant to induce a large PL position shift of a SWNT. Upon addition of FMN, SC on the (7,5) tube (Figure 9a) is slowly replaced with FMN wrapping, judging by the PL red-shift whose position approaches those of the FMN−SWNT dispersion. The PL intensity trajectory of the SC (7,5) tube (Figure 9b) displays two sigmoidal steps in which the first and second step intensities account for 33 and 67%, respectively. Assuming that the PL intensity of SC-wrapped *M*-(7,5) and *P*-(7,5) at the same concentration is similar, the ee value from 1 wt SC-dispersed (7,5) is 34%. A more detailed study of the determination of the ee of SC−SWNT dispersions will be published in the future.

This optical titration method using a chiral surfactant such as FMN and SC provides several advantages over the conventional method. In the conventional method, the determination of the ee of the SWNT is only useful when a sorted single-

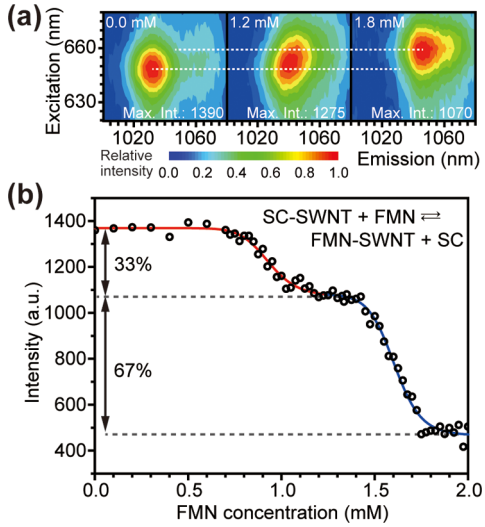

Figure 9. Determination of ee values of a SC-wrapped (7,5) nanotube against FMN. K_a differences in various SWNTs and origin of *P*-SWNT. (a) Series of representative PLE maps from the SC−HiPco sample with an increasing FMN concentration (0.00, 1.20, and 1.80 mM from left to right, respectively). (b) SC−SWNT PL intensity trajectory of (7,5) tubes.

chirality SWNT is prepared because of the complicated CD originating from multiple optical transitions.[17] In addition, the conventional method requires demanding surfactant exchange and subsequent dialysis steps with an achiral surfactant,[10] which is required to eliminate the effect of the chiral surfactant on the CD signal of the SWNT. Moreover, typical CD equipment that is optimized to analyze the structure of the protein in the UV region over the visible region typically takes several hours to acquire the visible spectrum even with a highly concentrated sample because of the weak CD activity of the SWNT [i.e., an enriched (6,5) sample with an absorbance of 2.0 at E_{11} results in CD activity with a weak signal (e.g., 20 mdeg) at E_{22}].[15] Lastly, the CD activity of the conventional method is presented as a normalized value against absorbance because of the lack of a pure handed SWNT.[17] On the other hand, our method is based on the PL activity of the SWNT being much stronger than the CD activity. Our method typically requires a few hours

DOI: 10.1021/acs.langmuir.7b02848
Langmuir 2017, 33, 11000−11009

(i.e., 4 min/PLE map, corresponding to 30 PLE maps in our setup) to determine ee values of entire SWNTs at once, which cannot be done as part of the conventional method, and takes several minutes to run a similar experiment with a single-chirality sample. If a titrant surfactant with a higher affinity for the SWNT is utilized and replaced with a dispersing surfactant,[25] this method does not have any distortion originating from sample preparation involving surfactant exchange and/or dialysis and SWNT bundling. Because of the higher PL activity, the titration measurement requires a quantity of a few milliliters with a diluted SWNT sample. We suspect that there might be weakness such as ambiguity upon assignment of SWNT handedness that proceeded by titration using another chiral surfactant, despite our result that the *P*-FMN helix displays a higher affinity with the *M*-SWNT.

CONCLUSION

The ee determination scheme was devised using chiral and achiral surfactant replacements using different binding affinities of the SWNT isomer for readily available chiral FMN caused by symmetry breaking. In addition, a SWNT wrapped with FMN exerts different effects on PL position according to SWNT modality and handedness, and its PL shift behavior is explained by unidirectional torsion of the FMN helix. Using a PLE-based optical titration assay using an achiral titrant, nanotubes wrapped by FMN show distinct blue-shifted PL with two-step PL intensity increases. The binding affinity between FMN and SWNT decreases with an increase in FMN concentration because of the disrupted $\pi-\pi$ interaction. The optimal FMN concentration results in a high binding affinity for an enantiomerically selective SWNT, preferring one SWNT handedness. Two PL steps were utilized to establish the absolute ee value of various (n,m) chiralities at once. The ee determination of the SC−SWNT dispersion also demonstrated the general usability of this method. The CD measurement-free, FMN-assisted ee determination method resembles the use of a chiral resolving agent in the field of organic chemistry.[37] This study delineates the general concept of cooperative interplay between the structure of the SWNT and the chiral surfactant that will be useful for the SWNT sorting scheme. This method provides an understanding of the optical properties for correlated SWNT modality and handedness behavior, which opens up the possibility of biosensory schemes and asymmetric nanocatalysts. This method allows the facile ee determination of a SWNT ensemble sample at once.

METHODS

Materials and Instrumentation. Flavin mononucleotide (FMN, lot 77623, purity of 72−75%), SDBS (technical grade), and SC were purchased from Sigma-Aldrich. Spectroscopic grade deionized water was obtained from Alfa Aesar. SWNTs prepared by a high-pressure carbon monoxide process [HiPco, raw grade, batch R1-831, with a diameter (d_t) distribution of 1.00 ± 0.35 nm] were purchased from Nanointegris. The atomistic structure of the FMN−SWNT dispersion was generated and visualized by Materials Studio (Biovia). UV−vis−NIR absorption spectra were acquired with either a Cary 5000 spectrometer or a JASCO 770 spectrometer with a cuvette having a 10 mm beam path unless otherwise noted.

FMN− and SC−HiPco Dispersions. To a mixture of 1 mg of SWNT and 4 mL of H_2O were added varying amounts of FMN (i.e., 1, 2, 4, 8, 32, 64, and 128 mg) to produce dispersions termed 1:4:*X* protocols, according to a previously published report.[20] Each dispersion was probe-sonicated (VCX 750, Sonics & Materials) for 2 h at 300 W. The resulting dark-greenish dispersion was centrifuged at 20000*g* for 2 h using an ultracentrifuge (Supra 22K, Hanil), and the supernatant (top 90%) was carefully collected. The SC−SWNT dispersion was prepared as follows. SC (1 wt %) was added to a mixture of 1 mg of HiPco and 2 mL of water, and the resulting mixture was subjected to the probe sonication described above for 1 h. The resulting dispersion was centrifuged at 15000*g* for 1.5 h; 80% supernatant was collected and further diluted 5-fold. This dispersion was titrated against FMN concentration using the PLE setup.

PLE Measurement and Titration. Fluorescence spectroscopy measurements were taken on a Spex Nanolog 3-211 spectrofluorometer equipped with a single-channel InGaAs detector and an iHR320 spectrometer with a 150 lines/mm grating. Titration of the FMN−SWNT dispersion (3 mL) was conducted by increasing the SDBS concentration in intervals as small as 25 μM prior to collection of the PLE map, according to the previous work.[25] Both excitation and emission light intensities were corrected against instrumental variations using sensitivity correction factors. In the case of the SC−HiPco titration, as little as 25 μM FMN was used as a titrant and the resulting map was collected.

CD Measurement. *CD Samples with Different ee Values.* Samples were prepared according to the following method. A portion of the FMN−SWNT sample was first titrated against SDBS at 0.45 and 0.8 mM. Sample 1 containing *M*-(8,6) was prepared by 0.8 mM SDBS titration. The supernatant was collected after addition of 0.5 M NaCl and subsequent centrifugation at 3000*g* for 10 min, according to a previous report.[20] Samples 2 were prepared similarly after a similar NaCl addition and subsequent 3000*g* centrifugation.

Removal of Extra FMN. To prepare the FMN-free SDBS−SWNT sample, 5 mM SDBS was added to the samples described above followed by dialysis against a 5 mM SDBS solution using dialysis tubing (molecular weight cutoff of 3000−5000) to remove the majority of FMN and NaCl in excess. The sample was further concentrated using a centrifugation-assisted Amicon tube. The subsequent absorption and PL spectra of the samples were measured to ensure that there was no measurable FMN residue. CD spectra were recorded with a JASCO 815 instrument with a 150 W xenon lamp as an excitation light source. Prior to measurement, each sample was equilibrated at 20 °C for ≥20 min to ensure tight thermal control.

Relative Binding Affinity Using the Hill Equation. A PLE map array was imported to generate concentration-dependent traces of PL intensity using the previously determined (n,m) position of carbon nanotubes.[20] PL intensity ρ is defined by the equation $\rho = [\mathrm{SDBS}]^{\gamma}/(K_a^{\gamma} + [\mathrm{SDBS}]^{\gamma})$. Sigmoidal transition curve fitting, relative binding affinity K_a, and the resulting Hill coefficient γ were obtained using the Hill function implemented in Origin.

ASSOCIATED CONTENT

Supporting Information

The Supporting Information is available free of charge on the ACS Publications website at DOI: 10.1021/acs.langmuir.7b02848.

Absorption spectra of varying FMN concentrations with the same amount of HiPco SWNTs and water concentration (Figure S1), a series of PLE maps of SWNTs dispersed by varying FMN concentrations (Figure S2), additional PL position shifts of SWNT chiralities at increasing concentrations of both FMN and SWNT (Figure S3), PL position shifts of SWNT chiralities in the 1:4:4 protocol upon addition of FMN (Figure S4), optical transition changes of SWNT with mod 2 for *M*- and *P*-handedness (Figure S5), relative binding affinity of the nine remaining nanotube chiralities from Figure 5 (Figure S6), PLE maps of sample 1 and sample 2 (Figure S7), overall trends of K_a with error bars according to nanotube chirality, handedness, and sample protocol (Figure S8), details of nonlinear iodixanol layering and density (Table S1), and PLE-derived E_{11}

DOI: 10.1021/acs.langmuir.7b02848
Langmuir 2017, 33, 11000−11009

and E_{22} positions, K_a values with errors, and ee values based on two-step PL intensities, according to chiral SWNTs (Table S2) (PDF)

AUTHOR INFORMATION

Corresponding Author

*E-mail: syju@yonsei.ac.kr.

Author Contributions

J.S. and S.K. contributed equally to this work.

Notes

The authors declare no competing financial interest.

ACKNOWLEDGMENTS

This research was supported by the Basic Science Research Program through the National Research Foundation of Korea (NRF) funded by the Ministry of Education, Science and Technology (2017R1D1A1A09000589), and in part by the Yonsei University Future-Leading Research Initiative of 2016 (2016-22-0099).

REFERENCES

(1) Yang, L.; Han, J. Electronic Structure of Deformed Carbon Nanotubes. *Phys. Rev. Lett.* **2000**, *85* (1), 154−157.

(2) Cronin, S. B.; Swan, A. K.; Ünlü, M. S.; Goldberg, B. B.; Dresselhaus, M. S.; Tinkham, M. Measuring the Uniaxial Strain of Individual Single-Wall Carbon Nanotubes: Resonance Raman Spectra of Atomic-Force-Microscope Modified Single-Wall Nanotubes. *Phys. Rev. Lett.* **2004**, *93* (16), 167401.

(3) Capaz, R. B.; Spataru, C. D.; Tangney, P.; Cohen, M. L.; Louie, S. G. Hydrostatic pressure effects on the structural and electronic properties of carbon nanotubes. *Phys. Status Solidi B* **2004**, *241* (14), 3352−3359.

(4) Vercosa, D. G.; Barros, E. B.; Souza Filho, A. G.; Mendes Filho, J.; Samsonidze, G. G.; Saito, R.; Dresselhaus, M. S. Torsional instability of chiral carbon nanotubes. *Phys. Rev. B: Condens. Matter Mater. Phys.* **2010**, *81* (16), 165430.

(5) Hall, A. R.; An, L.; Liu, J.; Vicci, L.; Falvo, M. R.; Superfine, R.; Washburn, S. Experimental Measurement of Single-Wall Carbon Nanotube Torsional Properties. *Phys. Rev. Lett.* **2006**, *96* (25), 256102.

(6) Lee, J. A.; Kim, Y. T.; Spinks, G. M.; Suh, D.; Lepró, X.; Lima, M. D.; Baughman, R. H.; Kim, S. J. All-Solid-State Carbon Nanotube Torsional and Tensile Artificial Muscles. *Nano Lett.* **2014**, *14* (5), 2664−2669.

(7) Withey, P. A.; Vemuru, V. S. M.; Bachilo, S. M.; Nagarajaiah, S.; Weisman, R. B. Strain Paint: Noncontact Strain Measurement Using Single-Walled Carbon Nanotube Composite Coatings. *Nano Lett.* **2012**, *12* (7), 3497−3500.

(8) Cohen-Karni, T.; Segev, L.; Srur-Lavi, O.; Cohen, S. R.; Joselevich, E. Torsional electromechanical quantum oscillations in carbon nanotubes. *Nat. Nanotechnol.* **2006**, *1* (1), 36−41.

(9) Dresselhaus, M. S.; Dresselhaus, G.; Avouris, P. *Carbon Nanotubes: Synthesis, Structure, Properties and Applications*; Springer: Berlin, 2001.

(10) Peng, X.; Komatsu, N.; Bhattacharya, S.; Shimawaki, T.; Aonuma, S.; Kimura, T.; Osuka, A. Optically Active Single-Walled Carbon Nanotubes. *Nat. Nanotechnol.* **2007**, *2* (6), 361−365.

(11) Peng, X.; Komatsu, N.; Kimura, T.; Osuka, A. Improved Optical Enrichment of SWNTs through Extraction with Chiral Nanotweezers of 2,6-Pyridylene-Bridged Diporphyrins. *J. Am. Chem. Soc.* **2007**, *129* (51), 15947−15953.

(12) Peng, X.; Komatsu, N.; Kimura, T.; Osuka, A. Simultaneous Enrichments of Optical Purity and (n,m) Abundance of SWNTs through Extraction with 3,6-Carbazolylene-Bridged Chiral Diporphyrin Nanotweezers. *ACS Nano* **2008**, *2* (10), 2045−2050.

(13) Wang, F.; Dukovic, G.; Brus, L. E.; Heinz, T. F. The Optical Resonances in Carbon Nanotubes Arise from Excitons. *Science* **2005**, *308* (5723), 838−841.

(14) Green, A.; Duch, M.; Hersam, M. Isolation of single-walled carbon nanotube enantiomers by density differentiation. *Nano Res.* **2009**, *2* (1), 69−77.

(15) Ghosh, S.; Bachilo, S. M.; Weisman, R. B. Advanced Sorting of Single-Walled Carbon Nanotubes by Nonlinear Density-Gradient Ultracentrifugation. *Nat. Nanotechnol.* **2010**, *5* (6), 443−450.

(16) Liu, H.; Tanaka, T.; Kataura, H. Optical Isomer Separation of Single-Chirality Carbon Nanotubes Using Gel Column Chromatography. *Nano Lett.* **2014**, *14* (11), 6237−6243.

(17) Wei, X.; Tanaka, T.; Yomogida, Y.; Sato, N.; Saito, R.; Kataura, H. Experimental determination of excitonic band structures of single-walled carbon nanotubes using circular dichroism spectra. *Nat. Commun.* **2016**, *7*, 12899.

(18) Ju, S.-Y.; Abanulo, D. C.; Badalucco, C. A.; Gascón, J. A.; Papadimitrakopoulos, F. Handedness Enantioselection of Carbon Nanotubes Using Helical Assemblies of Flavin Mononucleotide. *J. Am. Chem. Soc.* **2012**, *134* (32), 13196−13199.

(19) Ziegler, K. J.; Schmidt, D. J.; Rauwald, U.; Shah, K. N.; Flor, E. L.; Hauge, R. H.; Smalley, R. E. Length-Dependent Extraction of Single-Walled Carbon Nanotubes. *Nano Lett.* **2005**, *5* (12), 2355−2359.

(20) Ju, S.-Y.; Doll, J.; Sharma, I.; Papadimitrakopoulos, F. Selection of Carbon Nanotubes with Specific Chiralities using Helical Assemblies of Flavin Mononucleotide. *Nat. Nanotechnol.* **2008**, *3* (6), 356−362.

(21) Ju, S.-Y.; Kopcha, W. P.; Papadimitrakopoulos, F. Brightly Fluorescent Single-Walled Carbon Nanotubes via an Oxygen-Excluding Surfactant Organization. *Science* **2009**, *323* (5919), 1319−1323.

(22) Yoon, U.; Lee, Y.; Jang, H.; Jang, M.; Kim, J. S.; Lee, H. S.; Im, S.; Boo, D. W.; Park, J.; Ju, S.-Y. Graphene Nanoribbons Formed by a Sonochemical Graphene Unzipping using Flavin Mononucleotide as a Template. *Carbon* **2015**, *81*, 629−638.

(23) Gao, Z.; Zhi, C.; Bando, Y.; Golberg, D.; Serizawa, T. Noncovalent Functionalization of Disentangled Boron Nitride Nanotubes with Flavin Mononucleotides for Strong and Stable Visible-Light Emission in Aqueous Solution. *ACS Appl. Mater. Interfaces* **2011**, *3* (3), 627−632.

(24) Lin, C. S.; Zhang, R. Q.; Niehaus, T. A.; Frauenheim, T. Geometric and Electronic Structures of Carbon Nanotubes Adsorbed with Flavin Adenine Dinucleotide: A Theoretical Study. *J. Phys. Chem. C* **2007**, *111* (11), 4069−4073.

(25) Oh, H.; Sim, J.; Ju, S.-Y. Binding Affinities and Thermodynamics of Noncovalent Functionalization of Carbon Nanotubes with Surfactants. *Langmuir* **2013**, *29* (35), 11154−11162.

(26) Bachilo, S. M.; Strano, M. S.; Kittrell, C.; Hauge, R. H.; Smalley, R. E.; Weisman, R. B. Structure-Assigned Optical Spectra of Single-Walled Carbon Nanotubes. *Science* **2002**, *298* (5602), 2361−2366.

(27) Tan, P. H.; Rozhin, A. G.; Hasan, T.; Hu, P.; Scardaci, V.; Milne, W. I.; Ferrari, A. C. Photoluminescence Spectroscopy of Carbon Nanotube Bundles: Evidence for Exciton Energy Transfer. *Phys. Rev. Lett.* **2007**, *99* (13), 137402.

(28) Chou, S. G.; Plentz, F.; Jiang, J.; Saito, R.; Nezich, D.; Ribeiro, H. B.; Jorio, A.; Pimenta, M. A.; Samsonidze, Ge. G.; Santos, A. P.; Zheng, M.; Onoa, G. B.; Semke, E. D.; Dresselhaus, G.; Dresselhaus, M. S. Phonon-assisted Excitonic Recombination Channels Observed in DNA-wrapped Carbon Nanotubes using Photoluminescence Spectroscopy. *Phys. Rev. Lett.* **2005**, *94* (12), 127402.

(29) Jang, M.; Kim, S.; Jeong, H.; Ju, S. Y. Affinity-Mediated Sorting Order Reversal of Single-Walled Carbon Nanotubes in Density Gradient Ultracentrifugation. *Nanotechnology* **2016**, *27* (41), 41LT01.

(30) Arnold, M. S.; Stupp, S. I.; Hersam, M. C. Enrichment of Single-Walled Carbon Nanotubes by Diameter in Density Gradients. *Nano Lett.* **2005**, *5* (4), 713−718.

DOI: 10.1021/acs.langmuir.7b02848
Langmuir 2017, 33, 11000−11009

(31) Arnold, M. S.; Green, A. A.; Hulvat, J. F.; Stupp, S. I.; Hersam, M. C. Sorting Carbon Nanotubes by Electronic Structure using Density Differentiation. *Nat. Nanotechnol.* **2006**, *1* (1), 60−65.
(32) Sim, J.; Oh, H.; Koo, E.; Ju, S.-Y. Effect of Tight Flavin Mononucleotide Wrapping and Its Binding Affinity on Carbon Nanotube Covalent Reactivities. *Phys. Chem. Chem. Phys.* **2013**, *15* (44), 19169−19179.
(33) Saito, R.; Dresselhaus, G.; Dresselhaus, M. S. Trigonal warping effect of carbon nanotubes. *Phys. Rev. B: Condens. Matter Mater. Phys.* **2000**, *61* (4), 2981−2990.
(34) Sharifi, R.; Samaraweera, M.; Gascón, J. A.; Papadimitrakopoulos, F. Thermodynamics of the Quasi-Epitaxial Flavin Assembly around Various-Chirality Carbon Nanotubes. *J. Am. Chem. Soc.* **2014**, *136* (20), 7452−7463.
(35) Liu, H.; Tanaka, T.; Urabe, Y.; Kataura, H. High-Efficiency Single-Chirality Separation of Carbon Nanotubes Using Temperature-Controlled Gel Chromatography. *Nano Lett.* **2013**, *13* (5), 1996−2003.
(36) Liu, H.; Nishide, D.; Tanaka, T.; Kataura, H. Large-Scale Single-Chirality Separation of Single-Wall Carbon Nanotubes by Simple Gel Chromatography. *Nat. Commun.* **2011**, *2*, 309.
(37) Parker, D. NMR Determination of Enantiomeric Purity. *Chem. Rev.* **1991**, *91* (7), 1441−1457.

DOI: 10.1021/acs.langmuir.7b02848
Langmuir 2017, 33, 11000−11009

Supporting Information

Absolute Enantiomeric Excess Determination of Carbon Nanotubes Ensemble by Symmetry Breaking using Optical Titration Method

Jinsook Sim,[†] *Somin Kim,*[†] *Myungsu Jang, Minsuk Park, Hyunkyu Oh, and Sang-Yong Ju**

Department of Chemistry, Yonsei University, Seoul 03722, South Korea

[†] Equally contributed to this work

* Correspondence E-mail: syju@yonsei.ac.kr

Table of contents..... S1
DGU preparation and measurements..... S2
PL and PLE measurements along tube depth. S2
Figure S1. Absorption spectra of varying FMN concentration with same amount of HiPco SWNTs and water concentration..... S3
Figure S2. A series of PLE maps of SWNTs dispersed by varying FMN concentrations. S3
Figure S3. Additional PL position shifts of SWNT chiralities as increasing both FMN and SWNT..... S4
Figure S4. PL position shifts of SWNT chiralities in 1:4:4 protocol with addition of FMN. S5
Figure S5. Optical transition changes of SWNT with mod 2 for *M*- and *P*-handedness. S6
Figure S6. Relative binding affinity of the remaining nine nanotube chiralities from Figure 6. ..... S7
Figure S7. PLE maps of sample 1, and sample 2. ..... S8
Figure S8. Overall trends of K_a with error bar according to nanotube chirality, handedness, and sample protocols. S8
Table S1. Details of nonlinear iodixanol layering and density. S9
Table S2. PLE-derived E_{11} and E_{22} positions, K_a values with error, and ee based on two-step PL intensities, according to chiral SWNTs. S10
Cited references. S11

DGU preparation and measurements. *Iodixanol nonlinear density gradient preparation*: An aqueous solution of iodixanol was used as density gradient medium. The nonlinear density gradient was prepared according to the adaptation of our previous method.[1] Briefly, stock solutions with various iodixanol concentrations (*i.e.*, 20.0, 21.0, 22.0, 23.5, 25.0, 26.0, 27.0, 28.5, 30.0, 35.0, 40.0, 60.0 w/v %) with 1 mM FMN were prepared to produce gradient density, as shown in Table S1. Density gradient layering was formed in a centrifuge tube (13.2 mL capacity, ultraclear thinwall tube, 14 mm × 89 mm, Beckman Coulter) by introducing the stock solutions with a blunt-needled syringe from the bottom, with a density range from 1.320 to 1.107. To create smooth gradient density, the tube was tilted by 50 degrees from the vertical and was allowed to be equilibrated by diffusion for 24 hr at room temperature. Refractive indices of each gradient without 1 mM FMN was measured according to the our previous work.[1] 1.755 mL of aqueous FMN-SWNT dispersion was premixed with 1.245 mL 60 w/v % iodixanol to produce 3.0 mL FMN-SWNT dispersion containing 25 w/v % iodixanol. 2.6 mL aliquot was carefully injected immediately above the 25 w/v% density layer of iodixanol. Subsequently, the resulting centrifuge tube was centrifuged at 80,000 *g* (gravitational acceleration, 9.8 m/s^2) for 20 hr using a swing-bucket rotor (SW41Ti, Optima LE-80K ultracentrifuge, Beckman Coulter) at 22°C. For the balance of centrifugation step and absorption background measurements, centrifuge tube containing identical density gradient layering was prepared without loading of SWNT.

PL and PLE measurements along tube depth. To investigate the PLE depth profile, custom-made optical components were used to focus the excitation lights and translator, according to the previous method.[1] Briefly, monochromatic light was focused by using a convex lens (*f* = 30 mm, AC254-030-A-ML, Thorlabs) and the z position of centrifugation tube was controlled in a 3 mm interval by a custom-made translator on the rail installed to the sample chamber of the PLE setup. Single excitation PL profile along depth was obtained by excitation of focused laser (635 nm, 1.0 mW, Thorlabs, CPS180) by using a convex lens (*f* = 300 mm, LA1484-A, Thorlabs).

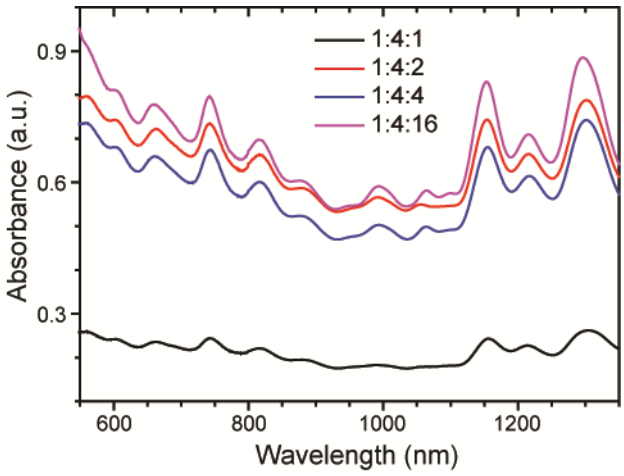

Figure S1. Absorption spectra of varying FMN concentration with same amount of HiPco SWNTs and water concentration.

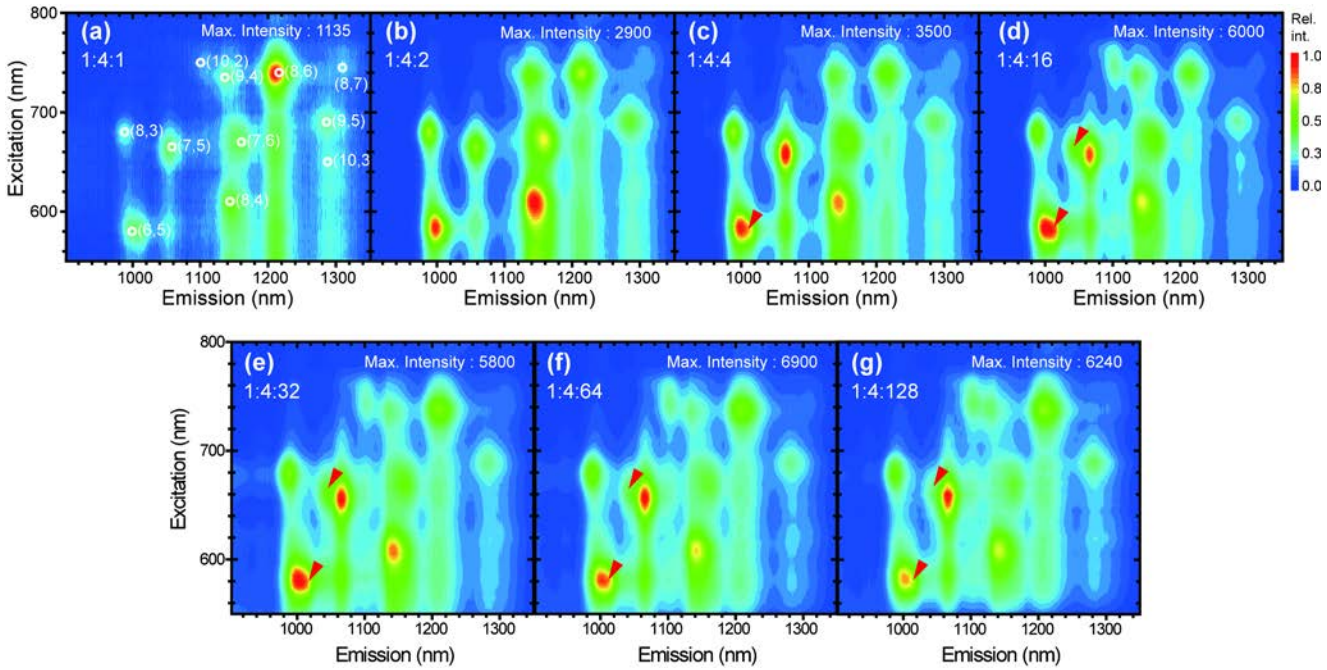

Figure S2. A series of PLE maps of SWNTs dispersed by varying FMN concentrations (1 mg of SWNT and 4 mL of water in the presence of 1, 2, 4, 16, 32, 64, and 128 mg of FMN). Note that the *P*-(6,5) peak emerges together with apparent *P*-(7,5) peak as increasing FMN concentration.

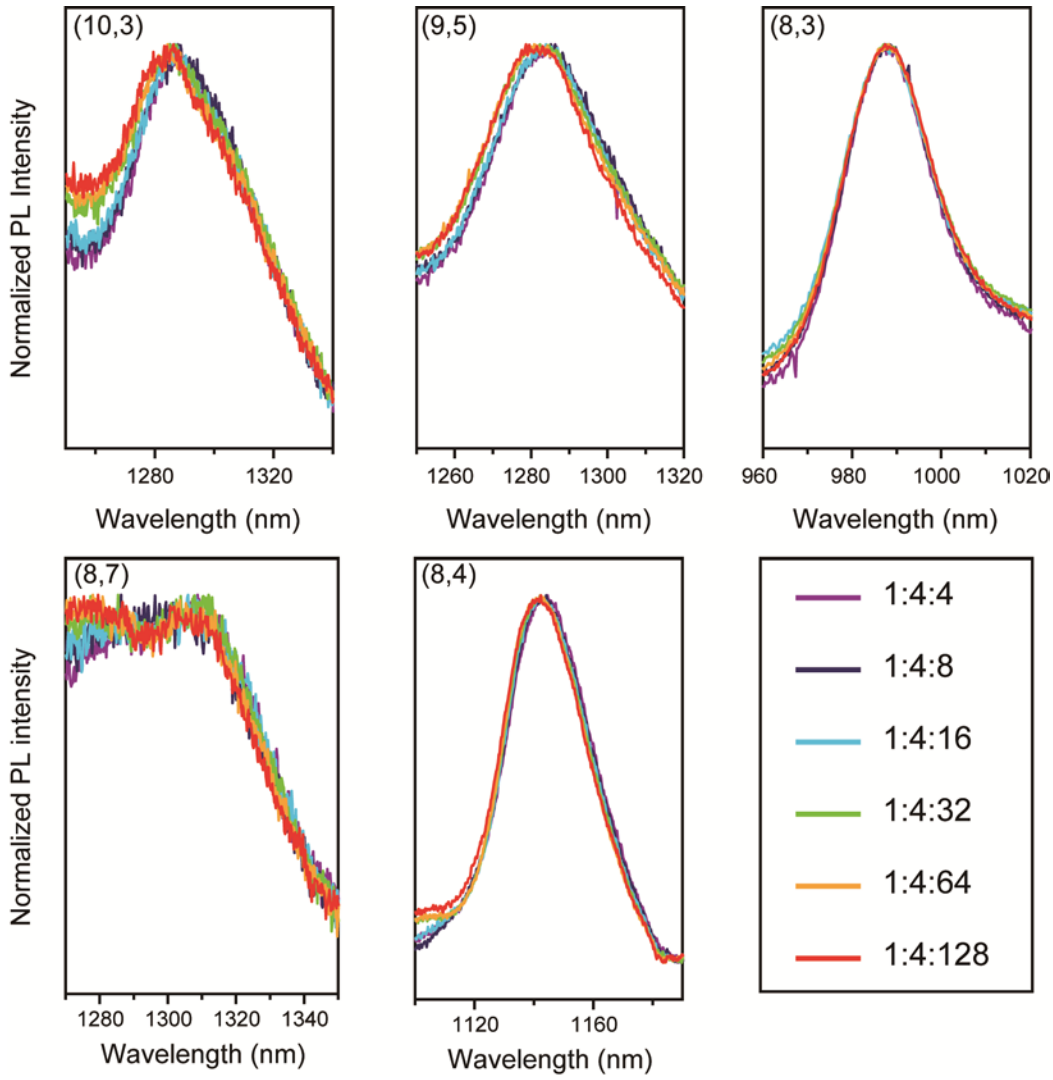

Figure S3. Additional PL position shifts of SWNT chiralities as increasing both FMN and SWNT.

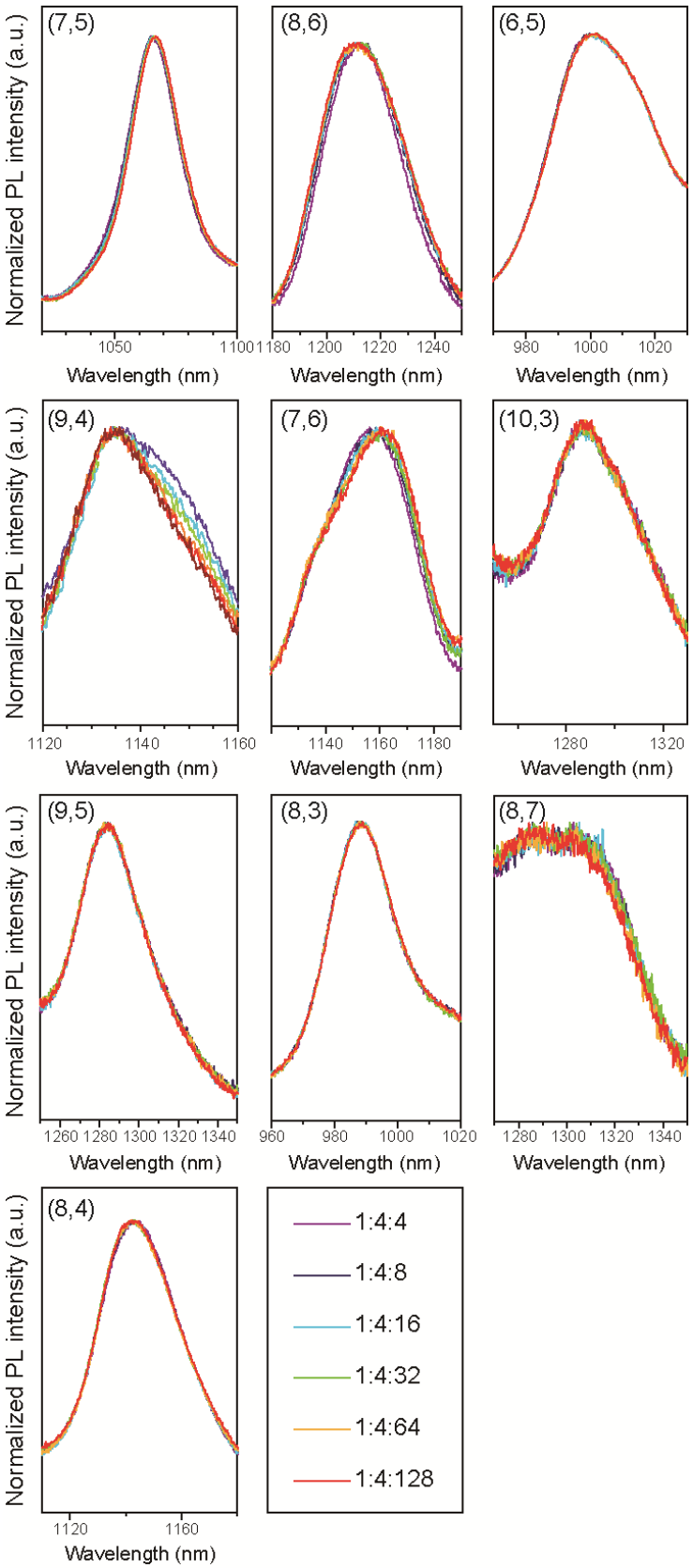

Figure S4. PL position shifts of SWNT chiralities in 1:4:4 protocol with addition of FMN.

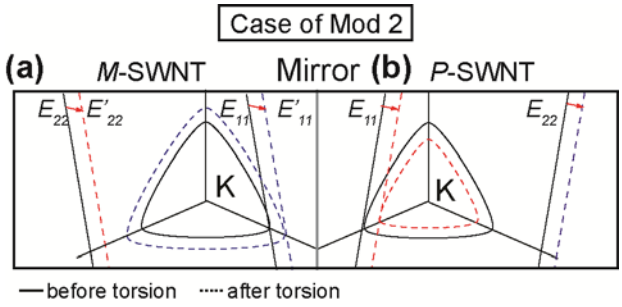

Figure S5. Optical transition changes of SWNT with mod 2 for (A) *M*- and (B) *P*-handedness.

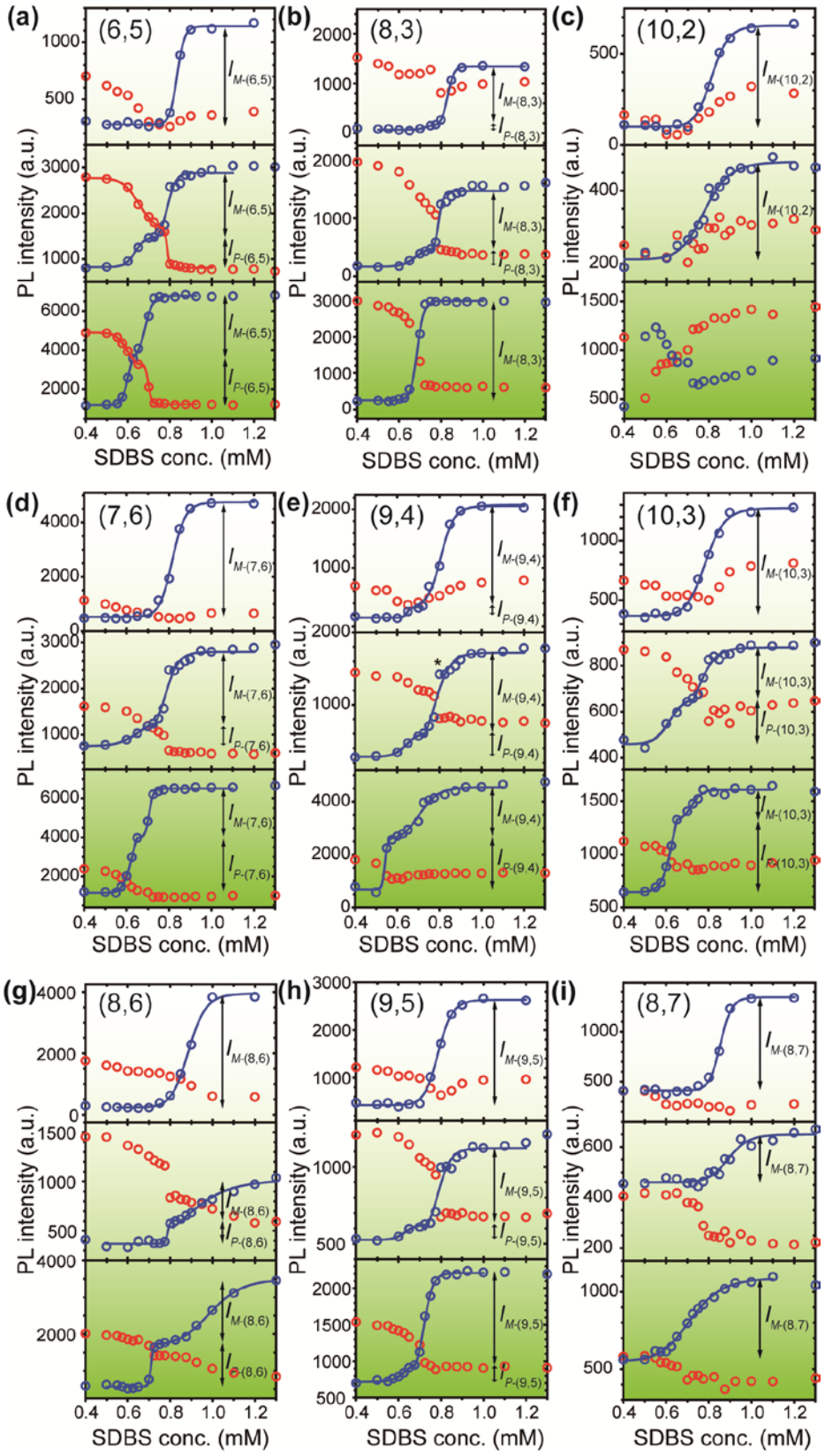

Figure S6. Relative binding affinity of the remaining nine nanotube chiralities from Figure 6. Each subset is obtained from 1:4:1, 1:4:4, and 1:4:16 protocols (top to bottom plots).

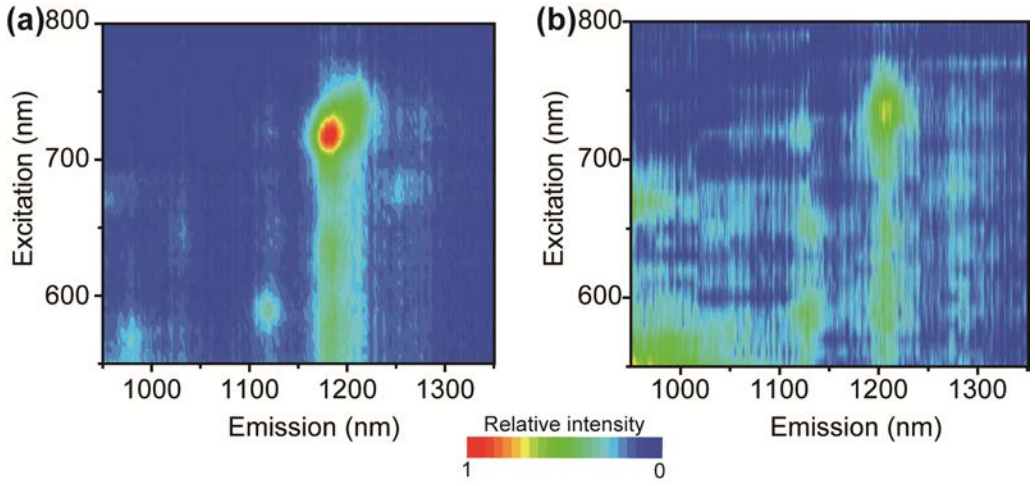

Figure S7. PLE maps of (a) sample 1, and (b) sample 2.

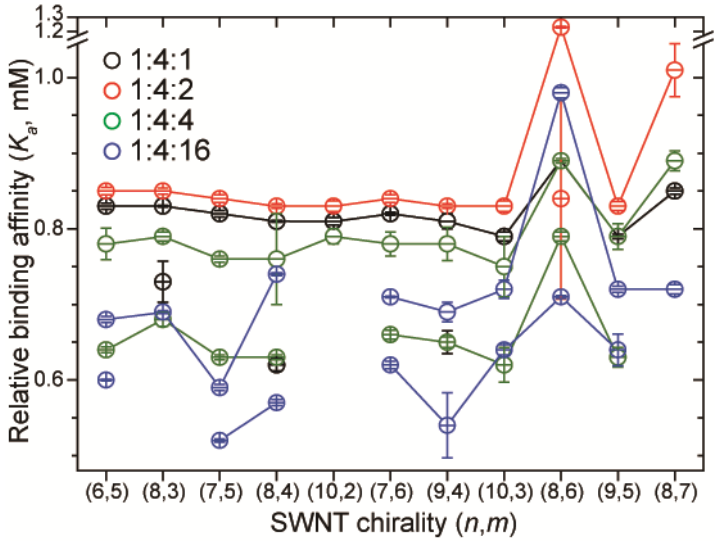

Figure S8. Overall trends of K_a with error bar according to nanotube chirality, handedness, and sample protocols.

Table S1. Details of nonlinear iodixanol layering and density.

Iodixanol content (w./v. %)	Density (g/cm^3)	Dilution (mL)		DGU (mL)
		60 w./v.% iodixanol	Water	
20.0	1.107	3.33	6.67	0.1
21.0	1.114	3.50	6.50	0.1
22.0	1.118	3.67	6.33	0.1
23.5	1.124	3.92	6.08	0.1
25.0	1.133	4.17	5.83	0.2
26.0	1.136	4.34	5.66	0.6
27.0	1.142	4.50	5.50	0.7
28.5	1.151	4.75	5.25	0.7
30.0	1.160	5.00	5.00	1.5
35.0	1.186	5.82	4.17	2.0
40.0	1.213	6.67	3.33	1.5
60.0	1.320	10.00	0.00	1.3

Table S2. PLE-derived E_{11} and E_{22} positions, K_a values with error, and ee based on two-step PL intensities, according to chiral SWNTs.

Assignment				PL position of FMN-HiPco				Dispersion protocol															
								1:4:1				1:4:2				1:4:4				1:4:16			
(*n*,*m*)	d_t [nm]	Chiral Angle[°]	Handed-ness	E^S_{11} [nm]	E^S_{22} [nm]	E^S_{11} [eV]	E^S_{22} [eV]	K_a [mM]	Error in K_a	γ	ee [%]	K_a [mM]	Error in K_a	γ	ee [%]	K_a [mM]	Error in K_a	γ	ee [%]	K_a [mM]	Error in K_a	γ	ee [%]
(6,5)	0.76	27	*P*	1009	579	1.23	2.14				100				100	0.64	0.004	25	36	0.60	0.001	41	12
			M	1004	585	1.24	2.12	0.83	0.004	47		0.85	0.005	35		0.78	0.021	21		0.68	0.004	36	
(8,3)	0.78	15.3	*P*	987	677	1.26	1.83	0.73	0.027	41	23				100	0.68	0.009	22	54				N/A
			M					0.83	0.001	56		0.85	0.004	36		0.79	0.006	71		0.69	0.002	43	
(7,5)	0.83	24.5	*P*	1058	658	1.17	1.88				100				100	0.63	0.003	21	64	0.52	0.002	56	24
			M	1067	656	1.16	1.89	0.82	0.004	26		0.84	0.005	49		0.76	0.004	57		0.59	0.004	42	
(8,4)	0.84	19.1	*P*	1146	605	1.08	2.05	0.62	0.008	28	89				100	0.63	0.003	24	22	0.57	0.004	29	1
			M					0.81	0.001	31		0.83	0.003	53		0.76	0.060	8		0.74	0.002	41	
(10,2)	0.88	8.9	N/A	1102	744	1.13	1.67	0.81	0.005	20	100	0.83	0.007	29	100	0.79	0.010	14	N/A				N/A
(7,6)	0.89	27.5	*P*	1160	670	1.07	1.85				100				100	0.66	0.006	13	60	0.62	0.005	30	6
			M					0.82	0.002	27		0.84	0.005	35		0.78	0.016	26		0.71	0.001	73	
(9,4)	0.92	17.5	*P*	1133	735	1.09	1.69	0.65	0.015	73	82				100	0.65	0.007	20	54	0.54	0.043	67	4
			M					0.81	0.010	26		0.83	0.003	48		0.78	0.022	22		0.69	0.013	10	
(10,3)	0.94	12.7	*P*	1288	651	0.96	1.91			18	100				100	0.62	0.023	17	8	0.64	0.007	23	42
			M					0.79	0.006			0.83	0.007	32		0.75	0.040	19		0.72	0.012	30	
(8,6)	0.97	25.3	*P*	1212	737	1.02	1.62			23	100	0.84	0.133	143	23	0.79	0.006	140	24	0.71	0.002	104	18
			M					0.89	0.003			1.23	0.005	21		0.89	0.003	4		0.98	0.007	9	
(9,5)	0.98	20.6	*P*	1286	689	0.96	1.80			24	100				100	0.63	0.013	25	66	0.64	0.021	20	68
			M					0.79	0.003			0.83	0.006	78		0.79	0.017	26		0.72	0.004	35	
(8,7)	1.03	27.8	N/A	1314	745	0.94	1.67	0.85	0.004	34	100	1.01	0.035	8	100	0.89	0.013	19	N/A	0.72	0.006	11	N/A

Cited references

1. Jang, M.; Kim, S.; Jeong, H.; Ju, S. Y., Affinity-Mediated Sorting Order Reversal of Single-Walled Carbon Nanotubes in Density Gradient Ultracentrifugation. *Nanotechnology* **2016,** *27* (41), 41LT01.